Optical Materials: X 12 (2021) 100106

Contents lists available at ScienceDirect

Optical Materials: X

journal homepage: www.journals.elsevier.com/optical-materials-x

Invited Article

Ultrafast luminescence of Ga- and In-doped ZnO ceramics

Piotr Rodnyi [a], Ivan Venevtsev [a,*], Elena Gorokhova [b], Sergei Eron'ko [b], Artem Chizhov [c], Faina Muktepavela [d]

[a] Peter the Great St. Petersburg Polytechnic University, 29 Polytechnicheskaya Street, St. Petersburg, 195251, Russia
[b] S.I. Vavilov State Optical Institute, 36 Babushkina Street, 192171, St. Petersburg, Russia
[c] Moscow State University, GSP-1, 1-3 Leninskiye Gory, Moscow, 119991, Russia
[d] Institute of Solid State Physics, University of Latvia, 8 Kengaraga Street, Riga, LV, 1063, Latvia

ARTICLE INFO

Keywords:
Zinc oxide
Scintillating ceramics
Near-band-edge emission
Radioluminescence
Total transmittance

ABSTRACT

In the presented work we compare luminescence characteristics of ZnO:Ga and ZnO:In ceramics prepared by hot uniaxial pressing method. Two types of initial powders were used. The first one was nanosized powder prepared by precipitation method. In the second case we used microsized powders and mechanical admixturing the oxides of intended dopant. In both cases doping by the trivalent ions lead to a significant quenching of ZnO visible emission and an increase in near-band-edge luminescence. The study has shown that the type of dopant greatly affects the transmittance of ceramics prepared from nano- and micro sized powders. Several reasons for the specific effect of powder preparation process and a type of introduced dopant, including changes in dopant solubility, their interaction with the grain boundaries, etc., were considered.

1. Introduction

The study of fast luminescence in scintillation materials is of great fundamental and applied importance [1,2]. Among ultrafast scintillators, materials based on ZnO [3] and BaF_2 [4] occupy a special place. In a great variety of ZnO materials (powders, crystals, ceramics) two types of luminescence bands are observed, namely, a narrow near UV band and a broad band in the visible spectral region. The UV band is located near the fundamental absorption edge of ZnO, therefore it is called near-band-edge (NBE) luminescence. This luminescence has an excitonic nature and shows a subnanosecond decay time [5]. The broad visible band results from electron recombination at luminescence centers, which are point defects, such as oxygen V_O [6,7] or zinc V_{Zn} [8] vacancies. This luminescence is characterized by a slow (microsecond range) decay time, which is undesirable for high-speed elements, in particular, for scintillators. The problem of suppressing visible band of luminescence and increasing the intensity of the ultrafast UV band may be solved by introducing trivalent ions Ga^{3+} [9], In^{3+} [10], Al^{3+} [11], and La^{3+} [12] into ZnO. The trivalent ions are usually incorporated into ZnO in the form of the corresponding oxides, which leads to a decrease in the number of oxygen vacancies and reduction of visible luminescence intensity, respectively. In addition, trivalent ions create donor levels, which causes an increase in the intensity of NBE luminescence [10]. The intensity of NBE luminescence can be increased also by annealing ZnO in various gases, in particular, in a hydrogen-containing atmosphere [13,14]. Effect of annealing in either Ar or O_2 ambient on luminescence characteristics of nanocrystalline films was studied in Ref. [15]. The Ar annealing of ZnO was found to be the ideal environment for the enhancement of NBE luminescence: a growth of ~40 times was achieved. The ratio of NBE to visible luminescence intensities increases 150-fold after thermal annealing for the undoped ZnO nanowire [16].

Origin of the NBE luminescence was extensively studied, but it is still in debate. Some authors suggested that the luminescence at room temperature (RT) originates from free exciton recombination [17,18]. However, it was reported that the most intense emission at RT for undoped crystal is related to bound excitons [19]. In some cases, the luminescence involves two different transitions, in which one is related to the ZnO free exciton and the other is related to the free-to-bound transition [20].

It should be noted that the study of the ZnO luminescence characteristics is carried out mainly on single crystals and films; less attention is paid to ceramics. In this paper, we focus on ZnO luminescence of undoped, Ga- and In-doped ceramics. To obtain a high NBE luminescence intensity and suppress the visible luminescence band, various conditions for the preparation of powders were applied (the temperature

* Corresponding author.
E-mail addresses: Piotr_Rodnyi@mail.ru (P. Rodnyi), Venevtsev.Ivan@gmail.com (I. Venevtsev).

https://doi.org/10.1016/j.omx.2021.100106
Received 9 June 2021; Received in revised form 15 October 2021; Accepted 18 October 2021
Available online 29 October 2021

and time of synthesis were varied). The original nano- and micro-sized powders were used to make ceramic samples, the characteristics of which were then compared. The optimal concentration of Ga and In impurities was chosen based on the results of our previous research [21].

2. Materials and methods

Nanosized powder samples were made by precipitation method from ZnO commercial microsized powders (Sigma Aldrich, 99% purity) [22]. Gallium and indium were added in a form of soluble salts before the actual precipitation. Final dopant concentration in case of Ga and In was 0.1 wt% and 0.13 wt% respectively. Five nanosized powders with the average grain size ranging from 30 to 40 nm have been made:

- undoped ZnO sintered in air at 600 °C during 60 h;
- ZnO:Ga 0.1 wt% sintered in air at 600 °C during 60 h;
- ZnO:In 0.13 wt% sintered in air at 600 °C during 60 h;
- ZnO:Ga 0.1 wt% sintered in air at 850 °C during 24 h;
- ZnO:In 0.13 wt% sintered in air at 850 °C during 24 h.

ZnO-based ceramics were prepared from the above-mentioned nanopowders. by uniaxial hot pressing in a high-temperature vacuum furnace (see e.g. Ref. [21]). The samples were obtained in the form of discs with a diameter of 24 mm and a thickness of 0.5 ÷ 1.0 mm (after polishing). We will designate the samples produced from nanopowders as *n-ceramics*.

In addition, Ga- and In-doped ceramic samples were made from commercial zinc oxide micro-sized powders, denoted as *m-ceramics.* The grain size of the initial powder in this case was from 50 × 50 nm^2 to 100 × 500 nm^2. Batches of different purity from various manufacturers were used. Doping of the m-ceramics was performed by mechanical admixture of Ga or In oxides.

Microstructure of all ceramics was studied using optical microscope. Infrared reflectance spectra were measured with an FCM-1201 FTIR spectrometer.

Total transmittance spectra in UV/Vis region were measured using SPECORD 200 PLUS double-beam spectrophotometer equipped with an integrating sphere.

Radioluminescence (RL) spectra were measured under continuous excitation using an X-ray tube with tungsten anode. The tube voltage and current were 40 kV and 10 mA, respectively. Emission was detected by an MDR-2 monochromator coupled to a Hamamatsu H8259-01 photon counting head. Samples were positioned in reflection geometry [23].

RL kinetics were measured under pulsed X-ray excitation (27 kV) using time correlated single photon counting. X-ray pulse width was

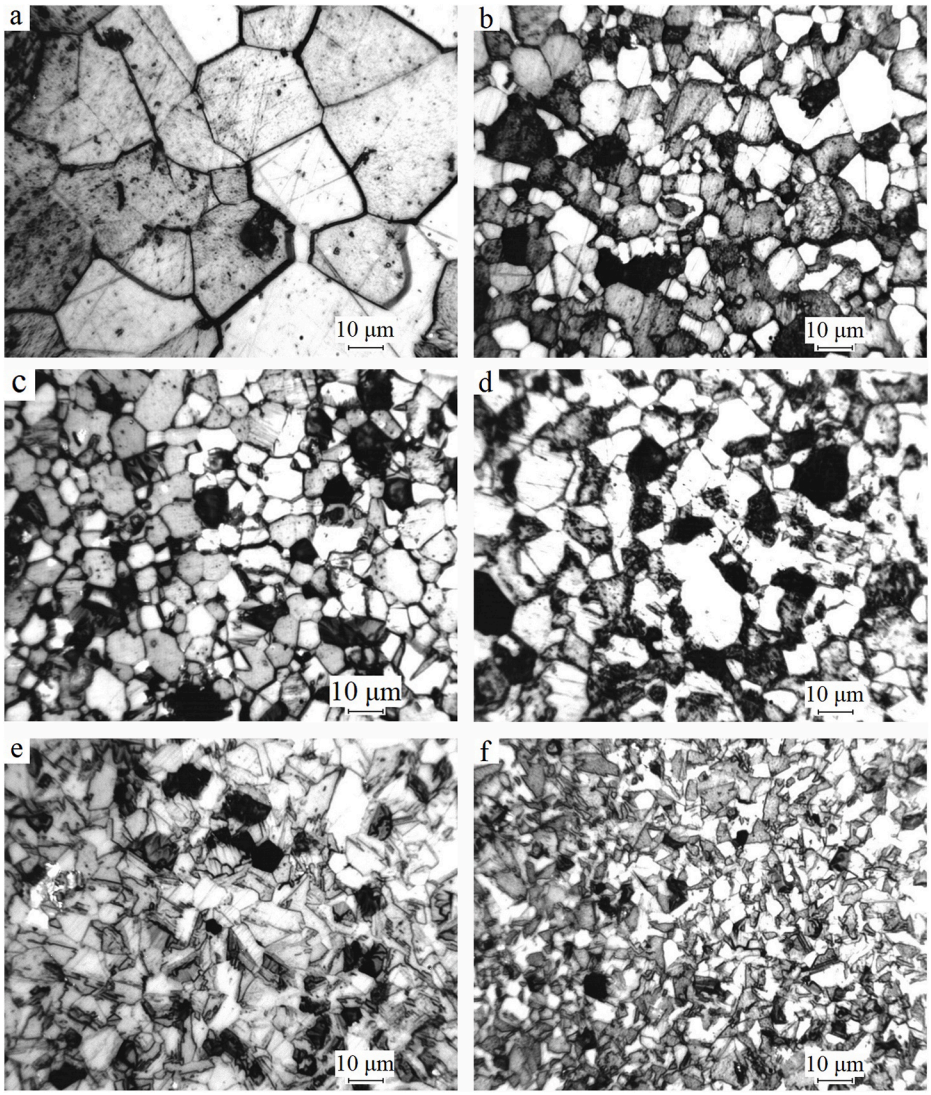

Fig. 1. Microstructure of (a) ZnO *m*-ceramics prepared straight from the commercial powder and ZnO n-ceramics prepared from the precipitated powders annealed in air at temperature (in brackets): (b) undoped ZnO powder (600 °C), (c) ZnO:Ga (600 °C), (d) ZnO:Ga (850 °C), (e) ZnO:In (600 °C), and (f) ZnO:In (850 °C).

around 800 ps with a maximum current of ~500 mA. This experimental setup is described in detail in Ref. [24].

3. Results

3.1. ZnO, ZnO:Ga, and ZnO:In ceramics prepared from nanoparticle samples

3.1.1. Microstructure

Microstructures of the obtained *n*-ceramics are shown in Fig. 1(b–f). A microphotograph of an undoped *m*-ceramics prepared from the initial microsized commercial powder is also shown for comparison (Fig. 1(a)). The microstructure of undoped ZnO ceramics in both *m*- and *n*-cases (Fig. 1 a and b, respectively) is composed of isometric grains, rounded grains and grains of an indefinite shape. The grain size of the *m*-ceramics ranges from 25 to 40 μm while in *n*-ceramics grains are considerably smaller: from 3 to 25 μm.

The introduction of Ga into ZnO leads to a decrease of grain size down to 4–16 μm with retention, slight deformation (or distortion) of isometric shape (Fig. 1(c and d)). Slight variation in grain size depending on the temperature of powder annealing was also observed. In case of the *n*-ceramics made of powders annealed at 850 °C, the appearance of grains of indefinite shape was registered.

In case of In doped *n*-ceramics (Fig. 1(e and f)) a drastic change in the shape of the grains was observed. The microstructure was predominated with elongated grains with jagged boundaries and grains of indefinite shape with sinuous boundaries. The average grain size varies from 2×8 to $5 \times 11 \div 15$ μm^2. Isometric grains were also present and had an average size of 5 μm. Increase in the powder annealing temperature lead to a slight decrease in a grain size.

3.1.2. Optical and luminescent properties

The results of measuring the total transmittance of the studied *n*-ceramics in the range from 350 to 1100 nm is shown in Fig. 2.

The transmittance curve of undoped *n*-ceramics is common for ZnO, except for the less steep absorption edge. All spectra have the absorption edge around 390–400 nm. Ga and In doped ceramics also exhibit a decrease in transmittance at wavelengths higher than 600 nm. All Ga doped ceramics have maximum transmittance around 18–20%. The ZnO:Ga (600 °C) ceramics also exhibit an increased absorption around 400–450 nm.

Indium doped ceramics demonstrate significantly better total transmittance. Increasing powder sintering temperature leads to a further rising of the total transmittance. The best result was obtained for ZnO:In (850 °C) ceramics where the total transmittance reached 32%. It should be noted that ZnO:Ga (850 °C) sample had a shorter-wavelength absorption edge (389 nm) compared to that of ZnO:In(850 °C) (397 nm).

Doping ZnO with trivalent Ga and In ions led to an increase of NBE emission intensity (Fig. 3) and significant quenching of the visible band. The best result was obtained for the ZnO:Ga (850 °C) ceramics which had its NBE luminescence intensity increased around 15 times compared to the undoped *n*-ceramics.

RL decay curves measured for all studied samples are shown in Fig. 4. Doped samples show predominantly fast components with a decay time about 0.7 ns (taking into account the width of the excitation pulse). All ceramics except ZnO:Ga (850 °C) exhibit a residual slow decay component. Ceramics which were obtained from powders, sintered at higher temperature have lower intensity of the visible band. The additional "bump" around 5–10 ns is an instrumental artifact which is localized and does not affect overall accuracy.

3.2. ZnO:Ga and ZnO:In ceramics prepared from commercial micro sized powders

3.2.1. Optical and luminescent properties

In *m*-ceramics, the same amount of dopants was introduced as in *n*-ceramics. Characteristic microstructures of *m*-ceramics are shown in Fig. 5. The microstructure of *m*-ZnO:Ga ceramics is composed of grains of an indefinite shape without a clear faceting with sinuous boundaries, as well as grains, the shape of which is close to isometric. The grain size (mainly) varies in the range of $5 \div 20$ μm, i.e. slightly larger than in *n*-cremics.

To compare with *m*-ceramics, two samples of *n*-ceramics (one Ga and one In doped) have been chosen. Both ZnO:Ga and ZnO:In *n*-ceramics were made of a powder annealed at 850 °C during 24 h and had higher transmittance and NBE emission intensity than other *n*-samples. Their total transmittance and RL spectra are shown in the same scale at Fig. 6 in comparison with spectra of *m*-ceramics of the same composition.

m-ZnO:Ga ceramics has lower NBE luminescence intensity (around 2.5 times) than the *n*-ZnO:Ga (850 °C) ceramics. ZnO:In *m*- and *n*-ceramics, on the contrary, had similar intensity of the NBE emission. It also should be noted that in Ga doped ceramics the visible band is more quenched than in In doped ones.

The maximum transmittance of the Ga and In doped *m*-ceramics is around 51 and 48%, respectively, which is higher than that of *n*-ceramics (15 and 32%, respectively). The absorption edge of ZnO:In *m*-ceramics lies at 392 nm, it is shifted to the short-wavelength region in comparison with that for similar *n*-ceramics, ~396 nm. Such shift was not observed in ZnO:Ga samples.

RL decay kinetics of *m*- and *n*-ceramics are shown at Fig. 7. The best ratio between fast and slow components was achieved for *n*-ZnO:Ga (850C). This corresponds to the fact that it had much lower intensity of the visible band (Fig. 6(a)). Other samples (*m*-ZnO:Ga and both ZnO:In) had quite similar distribution of slow and fast luminescent components.

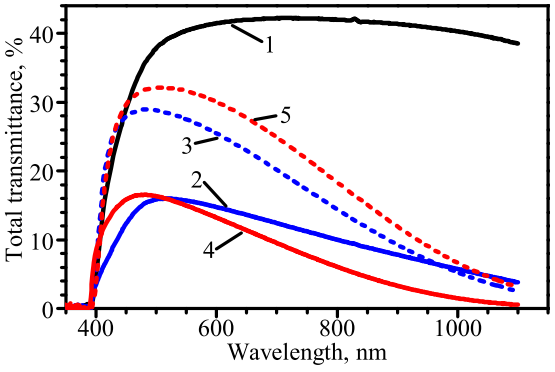

Fig. 2. Total transmittance of *n*-ceramics of 0.5 mm thickness. 1 – ZnO(600 °C), 2 – ZnO:Ga (600 °C), 3 – ZnO:In(600 °C), 4 – ZnO:Ga (850 °C), 5 – ZnO:In(850 °C).

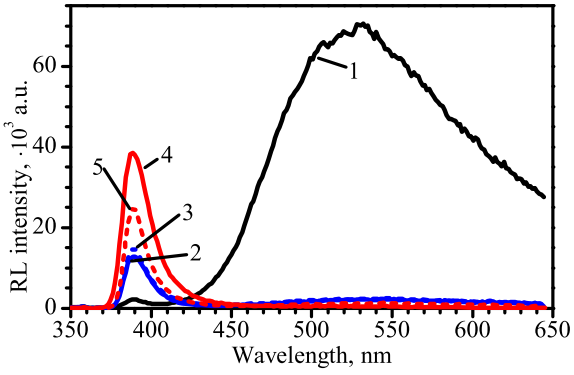

Fig. 3. Radioluminescence spectra of *n*-ceramics produced from undoped and Ga or In doped nanopowders: 1 – ZnO(600 °C), 2 – ZnO:Ga (600 °C), 3 – ZnO:In (600 °C), 4 – ZnO:Ga (850 °C), 5 – ZnO:In(850 °C).

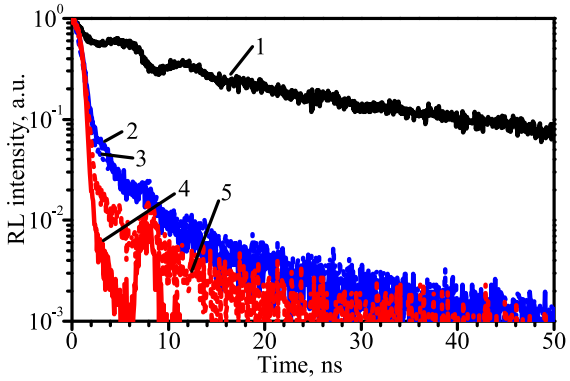

Fig. 4. Radioluminescence decay kinetics of *n*-ceramics: 1 – ZnO(600 °C), 2 – ZnO:Ga (600 °C), 3 – ZnO:In(600 °C), 4 – ZnO:Ga (850 °C), 5 – ZnO:In(850 °C).

3.2.2. *Infrared reflectance spectra*

The reflectance spectra of the ZnO:Ga and ZnO:In *m*- and *n*-ceramics in the long-wavelength region are presented in Fig. 8. The observed curve minima are due to the presence of free carriers generated by shallow donors resulting from the introduction of Ga or In Ref. [25]. As shown in Ref. [26], taking into account the effective mass of electrons, $0.24m_e$, and the high-frequency dielectric constant, 3.75, of ZnO, a simplified formula can be obtained for the electron concentration:

$$n = \frac{7.24 \cdot 10^{20}}{\lambda_{min}^2},$$

where λ_{min} is the wavelength of the minimum in the IR reflectance spectrum, expressed in microns; *n* is the concentration of free carriers in cm^{-3}.

The concentration of free carriers was determined based on the data obtained in the study of the reflection spectra of ZnO:Ga and ZnO:In ceramics in the mid-IR range (Fig. 8). Calculated values are presented in Table 1. The data obtained show that the concentration of free carriers in gallium ceramics is significantly higher than that of indium ceramics. The differences in the concentration of free carriers between *m*-ceramics and *n*-ceramics are not so significant. Nevertheless, the calculated values of the concentration of free carriers allow us to assume that the gallium content in *n*-ceramics is higher than in *m*-ceramics, and the indium content, on the contrary, is higher in *m*-ceramics.

4. Discussion

Microstructure of undoped ZnO *m*- and *n*-ceramics (Fig. 1(a) and (b), respectively) shows a significant effect caused by the morphology of the initial powder. Final grain size of the *n*-ceramics was more than twice smaller than that of the *m*-ceramics, although there were no significant changes in the shape of the grains. Smaller size could potentially lead to

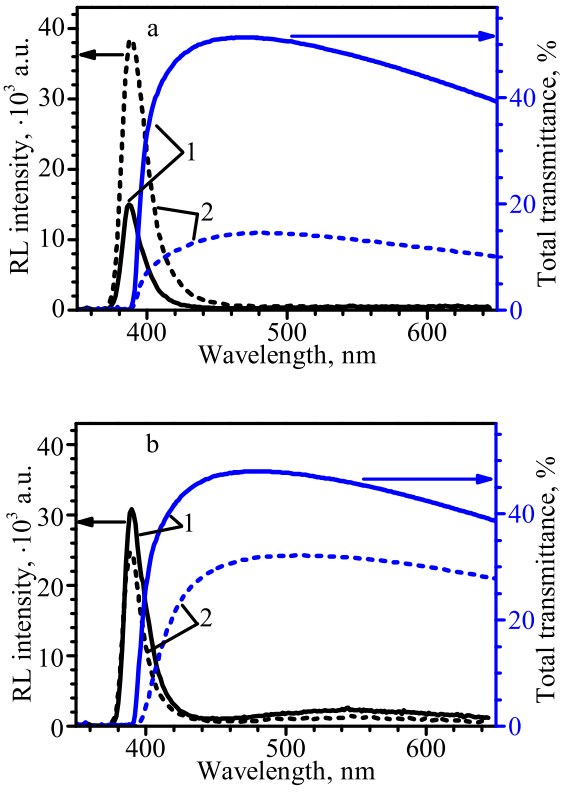

Fig. 6. Total transmittance and radioluminescence spectra of (a) ZnO:Ga and (b) ZnO:In. 1 – *m*-ceramics, 2 – *n*-ceramics (from powders annealed at 850 °C).

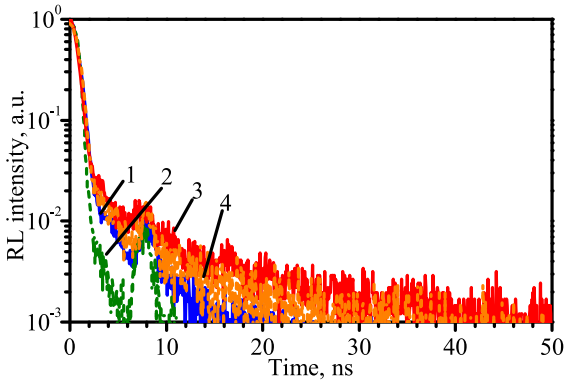

Fig. 7. Radioluminescence kinetics of 1 – *m*-ZnO:Ga, 2 – *n*-ZnO:Ga (850 °C), 3 – *m*-ZnO:In, and 4 – *n*-ZnO:In(850 °C) ceramics.

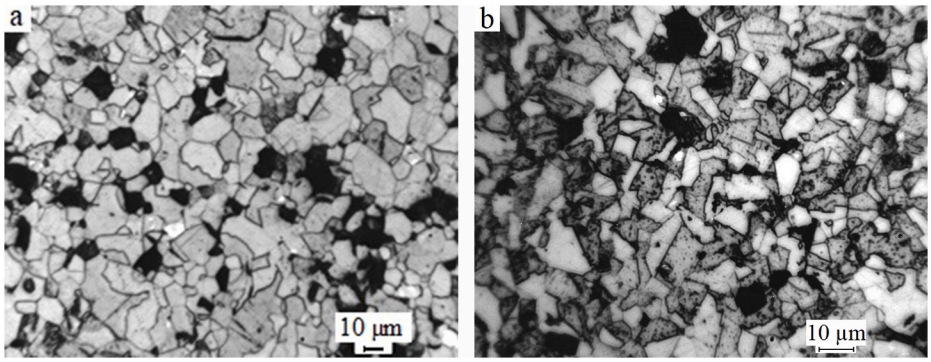

Fig. 5. Microstructure of (a) ZnO:Ga and (b) ZnO:In *m*-ceramics.

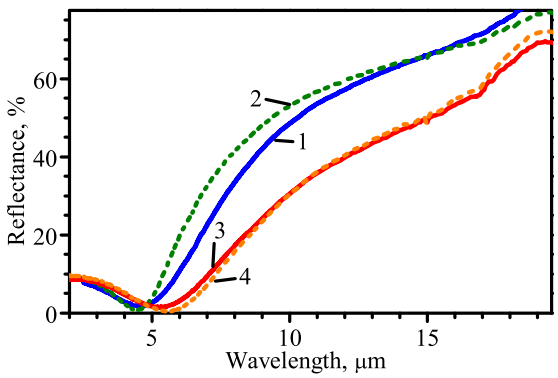

Fig. 8. Mid-IR reflectance spectra of 1 – *m*-ZnO:Ga, 2 – *n*-ZnO:Ga (850 °C), 3 – *m*-ZnO:In, and 4 – *n*-ZnO:In(850 °C) ceramics.

Table 1
Wavelength at the minimum of the reflectance spectrum, λ_{min}, and free carrier concentration *n* of ZnO:Ga and ZnO:In ceramics samples produced from microsized and nanosized powders.

Sample	*m*-ZnO:Ga	*n*-ZnO:Ga	*m*-ZnO:In	*n*-ZnO:In
λ_{min}, μm	4.6	4.5	5.25	5.5
n, cm^{-3}	$3.4{\cdot}10^{19}$	$3.6{\cdot}10^{19}$	$2.6{\cdot}10^{19}$	$2.4{\cdot}10^{19}$

a noticeable decrease in total transmittance due to a larger amount of refractive surfaces, pores, surface defects, etc.

Addition of dopants led to a further grain size decrease. In case of *n*-ZnO:Ga the final size of grains was 4–16 μm, which was only slightly smaller than of *m*-ZnO:Ga (Fig. 5(a)). Sintering a nanopowder at 850 °C instead of 600 °C also led to a small decrease in the average grain size. Indium dopant caused a drastic change in the ceramic morphology. In both *m*- and *n*-ceramics it caused a formation of elongated grains. Such behavior can be explained by the fact that indium is generally interacting at the grain boundaries. It leads to rounding of the initial faceted ZnO particles, which works in favor of the sintering process. At the stage of grain growth during hot pressing it promotes the formation of a characteristic microstructure of ceramics with jagged and zigzag grain boundaries [29]. Interestingly, this effect does not change with different method of impurity introduction.

Although the morphology of doped *m*- and *n*-ceramics was very close, their optical and scintillating characteristics showed significant differences. Ga doped *n*-ceramics had a much lower transmittance (less than 16%) than *m*-ceramics (51%). In doped *n*-ceramics (Fig. 2) had a transmittance around 28–32% which was still less that 48% of In doped *m*-ceramics. Increase in the powder sintering temperature from 600 °C to 850 °C led to an improvement of the total transmittance. Higher sintering temperature seems to have been a good choice since it also removed an absorption band which was present in ZnO:Ga (600 °C) *n*-ceramics (Fig. 2).

Presence of trivalent Ga and In ions in ZnO increased the intensity of NBE emission band (Fig. 3) and significantly quenched the visible band. The best result was obtained for the *n*-ZnO:Ga (850 °C) ceramics which had its NBE luminescence increased around 15 times compared to the undoped *n*-ceramics. The effect of powder sintering temperature was also observed in RL spectra. Increase in the sintering temperature resulted in an increase of the NBE emission intensity. The effect was much more pronounced in ZnO:Ga, in which an NBE emission increased three times, while in ZnO:In it only doubled. From RL spectra we cannot directly indicate which of the impurities is better. In case of ceramics made of precipitated powder, *n*-ZnO:In(600 °C) has only slightly higher NBE emission intensity than *n*-ZnO:Ga (600 °C). On the other hand, if powders were sintered at 850 °C, Ga doping has been undoubtedly better at quenching the visible band and increasing the NBE luminescence intensity.

For comparison with *m*-ceramics we have chosen *n*-ceramics produced from 850 °C annealed powder. Fig. 6 shows that even in case of In doping, a value of total transmittance of *n*-ceramics is still lower than of *m*-ceramics. On the other hand, ZnO:Ga *n*-ceramics clearly showed NBE emission intensity at least twice as high as in the *m*-ceramic.

Decay kinetics at Figs. 4 and 7 indicate that successful quenching of slow visible component was achieved in all *m*- and *n*-ceramics, especially in ZnO:Ga (850 °C) which had the lowest relative intensity of the slow emission. In doping was a bit less effective, but still decreased a slow component emission intensity at least 10 times.

The difference in the total transmittance of *n*- and *m*-ceramics can be associated with the different grain size of the initial powders. The use of nanopowders with high adsorption activity in the hot pressing process could have led to a decrease in the level of transparency.

Differences observed in the RL intensity and transmittance of Ga and In doped ZnO ceramics could also have been caused by a number of other reasons. Firstly, the position occupied by the impurity ion in the crystal structure is important. Since the effective ionic radii of Ga^{3+} both at tetrahedral (0.47 Å) and octahedral (0.62 Å) coordination are less than those of Zn^{2+} (0.62 and 0.74 Å, respectively [27]), it can occupy regular positions in the wurtzite structure, replacing zinc ions with tetrahedral coordination, or introduce itself into octahedral interstitials. This, in particular, is mentioned in the works devoted to the study of ZnO:Ga films [28,29]. Indium, which has the effective ionic radius (0.80 Å for octahedral coordination) greater than that of Zn^{2+} (0.74 Å), can be localized at the grain boundaries [10].

Secondly, differences in the RL intensities of the ceramics produced from nano- and micropowders could be caused by different doping methods. In the case of using mechanical admixture, the formation of a luminescent material occurs directly during the hot pressing process, i.e. by solid-phase synthesis, which is characterized by limited solubility of Ga and In (up to 0.3–0.5 at.%) [30,31]. With solution-based methods of synthesis, an increase in the solubility limit is observed, in particular, up to 2 at.% of Ga [31]. Therefore, despite the same amount of the introduced dopant, the concentration in the final product (in the ceramics) can be different.

Finally, some of the observed properties can be explained with the help of IR reflectance spectra. The data of Table 1 show that indium doping resulted in lesser concentration of free carriers than gallium doping. This is supported by the fact that added content of In, expressed in atomic percent (0.046 at.%) is smaller than added content of Ga (0.058 at.%). Such difference corresponds to the worse quenching of visible luminescence component in In containing ceramics.

The ratio of added Ga/In in *m*- and *n*-ceramics (1.3) is slightly less than the ratio between respective concentrations of free carriers (1.3–1.5). Considering that concentration of free carriers has to be somewhat proportional to the amount of Ga and In ions dissolved in the ZnO (at least at low concentrations), one can assume that solubility of In is less than that of Ga. That results in a decreased RL intensity of *n*-ZnO:In compared with *m*-ceramics. This may be an indirect confirmation of the statement that indium is more likely to remain at the grain boundaries, while gallium is better embedded in the crystal lattice. We suppose that simultaneous doping with Ga and In may utilize advantages of both dopants and lead to further improvement of ceramics optical and scintillating properties.

In terms of performance, one should consider a spectral overlap between NBE emission and total transmittance. If a future application requires a sample with high thickness, that overlap would be the crucial parameter since it directly affects the amount of light escaping the scintillator. In that regard an In doped *m*-ceramics will have the best performance since it has higher NBE emission intensity than ZnO:Ga *m*-ceramics and its absorption edge is not shifted to longer wavelengths as in *n*-ZnO:In(850 °C). If a scintillator has to be thin or the detector has a "reflection" geometry, than the best option would be *n*-ZnO:Ga (850 °C) ceramics which has significantly higher NBE emission intensity.

5. Conclusions

The study of the ceramics produced from precipitated nanosized powders showed that doping of the ZnO with trivalent ions leads to an increase of the NBE emission intensity and significant quenching of the visible band. All doped ceramic samples showed predominantly fast luminescence in the spectral range from 380 to 410 nm with the decay time of 0.7 ns, which is suitable for applications requiring high speed counting.

Ceramics produced from precipitated powder, annealed at higher temperatures, generally showed better performance than ceramics annealed at lower temperatures. Indium doping resulted in higher transmittance than gallium doping due to its specific interaction with grain boundaries during hot pressing. This is supported by microstructures and IR reflectance measurements. Introduction of Ga, on the other hand led to stronger NBE luminescence band and better quenching of the visible component. Other possible reasons which may explain differences include difference in ionic radii of dopants and the positions they prefer to occupy in the crystal lattice or different solubility of dopants, depending on the powder preparation method. Here we conclude that simultaneous Ga and In doping is one of possible ways to further improve ZnO based scintillators.

Currently the best result in terms of NBE intensity was obtained for ZnO:Ga (850 °C) ceramics made of precipitated nanosized powder, which might be applicable in cases where transmittance is not of the first importance. ZnO:In ceramics made of commercial microsized powder performed better in terms of total transmittance and its spectral overlap with NBE emission. It should be noted that in the first trial experiment [32], ZnO:In ceramics with a thickness of 1.0 mm made of microsized powders showed good characteristics in detecting heavy ions.

CRediT authorship contribution statement

Piotr Rodnyi: Writing – review & editing, Funding acquisition, Supervision. **Ivan Venevtsev:** Investigation, Writing – original draft, Writing – review & editing, Visualization. **Elena Gorokhova:** Investigation, Resources, Writing – review & editing, Visualization. **Sergei Eron'ko:** Investigation. **Artem Chizhov:** Resources. **Faina Muktepavela:** Writing – review & editing.

Declaration of competing interest

The authors declare that they have no known competing financial interests or personal relationships that could have appeared to influence the work reported in this paper.

Acknowledgements

The work of authors (a-c) was financially supported by Russian Foundation for Basic Research (RFBR, Russia) and the work of the last author (d) had financial support from State Education Development Agency (VIAA, Latvia). All of that was approved as a result of ERA.Net RUS PLUS 2017 joint call for proposals. Here is the link for the joint call for reference: https://www.eranet-rus.eu/en/196.php.

References

[1] G. Blasse, Scintillator materials, Chem. Mater. 6 (9) (1994) 1465–1475, https://doi.org/10.1021/cm00045a002.
[2] C. Ronda, H. Wieczorek, V. Khanin, P. Rodnyi, Review - scintillators for medical imaging: a tutorial overview, ECS J. Solid State Sci. Technol. 5 (1) (2016) R3121–R3125, https://doi.org/10.1149/2.0131601jss.
[3] H. Nanto, M. Sato, Yu Miyamoto, K. Hirasawa, Yoshinori Takei, T. Yanagida, T. Nakamura, M. Katagiri, Luminescence properties of impurity-doped zinc oxide phosphor for novel neutron detection, Sensor. Mater. 28 (8) (2016) 905–916, https://doi.org/10.18494/SAM.2016.1251.
[4] V.V. Vistovskyy, A.V. Zhyshkovych, O.O. Halyatkin, N.E. Mitina, A.S. Zaichenko, P. A. Rodnyi, A.N. Vasil'ev, A.V. Gektin, A.S. Voloshinovskii, The luminescence of BaF_2 nanoparticles upon high-energy excitation, J. Appl. Phys. 116 (2014), 054308, https://doi.org/10.1063/1.4892112.
[5] J. Ji, A.M. Colosimo, W. Anwand, L.A. Boatner, A. Wagner, P.S. Stepanov, T. T. Trinh, M.O. Liedke, R. Krause-Rehberg, T.E. Cowan, F.A. Selim, ZnO luminescence and scintillation studied via photoexcitation, X-ray excitation and gamma-induced positron spectroscopy, Sci. Rep. 6 (2016) 31238, https://doi.org/10.1038/srep31238.
[6] Y. Wang, B. Yang, N. Can, P.D. Townsend, Correlations between low temperature thermoluminescence and oxygen vacancies in ZnO crystals, J. Appl. Phys. 109 (2011), 053508, https://doi.org/10.1063/1.3556743.
[7] P.A. Rodnyi, K.A. Chernenko, I.D. Venevtsev, Mechanisms of ZnO luminescence in the visible spectral region, Opt Spectrosc. 125 (3) (2018) 372–378, https://doi.org/10.1134/S0030400X18090205.
[8] H. Chen, S. Gu, K. Tang, S. Zhu, Zh Zhu, J. Ye, R. Zhang, Y. Zheng, Origins of green band emission in high-temperature annealed N-doped ZnO, J. Lumin. 131 (6) (2011) 1189–1192, https://doi.org/10.1016/j.jlumin.2011.02.025.
[9] T. Makino, Y. Segawa, S. Yoshida, A. Tsukazaki, A. Ohtomo, M. Kawasaki, Gallium concentration dependence of room-temperature near-band-edge luminescence in n -type ZnO:Ga, Appl. Phys. Lett. 85 (5) (2004) 759–761, https://doi.org/10.1063/1.1776630.
[10] L. Grigorjeva, J. Grube, I. Bite, A. Zolotarjovs, K. Smits, D. Millers, P. Rodnyi, K. Chernenko, Sub-nanosecond excitonic luminescence in ZnO:In nanocrystals, Radiat. Meas. 123 (2019) 69–73, https://doi.org/10.1016/j.radmeas.2019.02.016.
[11] A. Mohanta, J.G. Simmons Jr., G. Shen, S.M. Kim, P. Kung, H.O. Everitt, Al doping in ZnO nanowires enhances ultraviolet emission and suppresses broad defect emission, J. Lumin. 211 (2019) 264–270, https://doi.org/10.1016/j.jlumin.2019.03.049.
[12] L. Prochazkova, T. Gbur, V. Cuba, V. Jary, M. Nikl, Fabrication of highly efficient ZnO nanoscintillators, Opt. Mater. 47 (2015) 67–71, https://doi.org/10.1016/j.optmat.2015.07.001.
[13] E.D. Bourret-Courchesne, S.E. Derenzo, M.J. Weber, Development of ZnO:Ga as an ultra-fast scintillator, Nucl. Instrum. Methods Phys. Res. A 601 (3) (2009) 358–363, https://doi.org/10.1016/j.nima.2008.12.206.
[14] P. Rodnyi, K. Chernenko, O. Klimova, V. Galkin, A. Makeenko, E. Gorokhova, D. Buettner, W. Keur, H. Wieczorek, Influence of annealing on the scintillation properties of zinc oxide powders and ceramics, Radiat. Meas. 90 (2016) 136–139, https://doi.org/10.1016/j.radmeas.2016.01.021.
[15] D. Thapa, J. Huso, J.L. Morrison, C.D. Corolewski, M.D. McCluskey, L. Bergman, Achieving highly-enhanced UV photoluminescence and its origin in ZnO nanocrystalline films, Opt. Mater. 58 (2016) 382–389, https://doi.org/10.1016/j.optmat.2016.05.008.
[16] H. Ghosh, B. Sadeghimakki, S. Sivoththaman, Enhancement of UV emission and optical bandgap of ZnO nanowires via doping and post-growth annealing, Mater. Res. Express 7 (3) (2020), 035013, https://doi.org/10.1088/2053-1591/ab77f0.
[17] L. Wang, N.C. Giles, Temperature dependence of the free exciton transition energy in zinc oxide by photoluminescence excitation spectroscopy, J. Appl. Phys. 94 (2) (2003) 973–978, https://doi.org/10.1063/1.1586977.
[18] Z.K. Tang, M. Kawasaki, A. Ohtomo, H. Koinuma, Y. Segawa, Self-assembled ZnO nano-crystals and exciton lasing at room temperature, J. Cryst. Growth 287 (1) (2006) 169–179, https://doi.org/10.1016/j.jcrysgro.2005.10.062.
[19] N. Ohashi, T. Ishigaki, N. Okada, T. Sekiguchi, I. Sakaguchi, H. Haneda, Effect of hydrogen doping on ultraviolet emission spectra of various types of ZnO, Appl. Phys. Lett. 80 (16) (2002) 2869–2871, https://doi.org/10.1063/1.1470703.
[20] Q.X. Zhao, M. Willander, R.E. Morjan, Q.-H. Hu, E.E.B. Campbell, Optical recombination of ZnO nanowires grown on sapphire and Si substrates, Appl. Phys. Lett. 83 (1) (2003) 165–167, https://doi.org/10.1063/1.1591069.
[21] K.A. Chernenko, E.I. Gorokhova, S.B. Eron'ko, A.V. Sandulenko, I.D. Venevtsev, H. Wieczorek, P.A. Rodnyi, Structural, optical, and luminescent properties of ZnO: Ga and ZnO:In ceramics, IEEE Trans. Nucl. Sci. 65 (8) (2018) 2196–2202, https://doi.org/10.1109/TNS.2018.2810331.
[22] N. Vorobyeva, M. Rumyantseva, D. Filatova, E. Konstantinova, D. Grishina, A. Abakumov, S. Turner, A. Gaskov, Nanocrystalline ZnO(Ga): paramagnetic centers, surface acidity and gas sensor properties, Sensor. Actuator. B Chem. 182 (2013) 555–564, https://doi.org/10.1016/j.snb.2013.03.068.
[23] A.S. Potapov, P.A. Rodnyi, S.B. Mikhrin, Experimental set-up for measurement of luminescence characteristics at X-ray excitation, Radiat. Meas. 38 (4–6) (2004) 839–842, https://doi.org/10.1016/j.radmeas.2004.02.007.
[24] P.A. Rodnyi, S.B. Mikhrin, A.N. Mishin, A.V. Sidorenko, Small-size pulsed X-ray source for measurements of scintillator decay time constants, IEEE Trans. Nucl. Sci. 48 (6) (2001) 2340–2343, https://doi.org/10.1109/23.983264.
[25] J.S. Neal, N.C. Giles, X. Yang, R.A. Wall, K.B. Ucer, R.T. Williams, D.J. Wisniewski, L.A. Boatner, V. Rengarajan, J. Nause, B. Nemeth, Evaluation of melt-grown ZnO single crystals for use as alpha-particle detectors, IEEE Trans. Nucl. Sci. 55 (3) (2008) 1397–1403, https://doi.org/10.1109/TNS.2008.922829.
[26] X.C. Yang, degree D.Ph. in Physics, Electrical and Optical Properties of Zinc Oxide for Scintillator Applications. Dissert, vol. 6, West Virginia Univ. Ch., Morgantown, USA, 2008, p. 168.
[27] R.D. Shannon, Revised effective ionic radii and systematic studies of interatomic distances in halides and chalcogenides, Acta Crystallogr. A. 32 (1976) 751–767, https://doi.org/10.1107/S0567739476001551.
[28] A.R. Kaul, O.Yu Gorbenko, A.N. Botev, L.I. Burova, MOCVD of pure and Ga-doped epitaxial ZnO, Superlattice. Microst. 38 (2005) 272–282, https://doi.org/10.1016/j.spmi.2005.08.004.
[29] S. Chen, G. Carraro, D. Barreca, A. Sapelkin, W. Chen, X. Huang, Q. Cheng, F. Zhange, R. Binions, Aerosol assisted chemical vapor deposition of Ga doped ZnO films for energy efficient glazing: effects of doping concentration on the film

growth behavior and optoelectronic properties, J. Mater. Chem. A. 3 (2015) 13039–13049, https://doi.org/10.1039/C5TA02163D.
[30] M.H. Yoon, S.H. Lee, H.L. Park, H.K. Kim, M.S. Jang, Solid solubility limits of Ga and Al in ZnO, J. Mater. Sci. Lett. 21 (2002) 1703–1704, https://doi.org/10.1023/A:1020841213266.
[31] H. Serier, A. Demourgues, M. Gaudon, Investigation of Ga substitution in ZnO powder and opto-electronic properties, Inorg. Chem. 49 (15) (2010) 6853–6858, https://doi.org/10.1021/ic1000733.
[32] P. Rodnyi, I. Venevtsev, E. Gorokhova, S. Eron'ko, P. Boutachkov, M. Saifulin, Fast, efficient, and radiation hard ZnO, in: In ceramic scintillator, 2019 IEEE International Conference on Electrical Engineering and Photonics (EExPolytech), 2019, pp. 197–200, https://doi.org/10.1109/EExPolytech.2019.8906846.

Institute of Solid State Physics, University of Latvia as the Center of Excellence has received funding from the European Union's Horizon 2020 Framework Programme H2020-WIDESPREAD-01-2016-2017-TeamingPhase2 under grant agreement No. 739508, project CAMART2.